Z. Phys. B 93, 365–373 (1994)

ZEITSCHRIFT
FÜR PHYSIK B

STM investigations of PTCDA and PTCDI on graphite and MoS_2. A systematic study of epitaxy and STM image contrast

C. Ludwig, B. Gompf, J. Petersen, R. Strohmaier, W. Eisenmenger

1. Physikalisches Institut, Universität Stuttgart, Pfaffenwaldring 57, D-70550 Stuttgart, Germany

Received: 22 June 1993 / Revised version: 27 July 1993

Abstract. Monolayers of the organic molecules perylene-3,4,9,10-tetra-carboxylic-dianhydride (PTCDA) and -di-imide (PTCDI) on graphite and MoS_2 have been imaged with scanning tunneling microscopy. The epitaxial growth of the two molecules is determined by the intermolecular interaction but nearly independent of the substrate. On both substrates the STM image contrast in the submolecularly resolved images is dominated by the aromatic perylene system whereas the polar oxygen and nitrogen groups are invisible. The correlation of the observed inner structure of the molecules to their molecular structure allows us to compare our results with theoretical considerations.

PACS: 61.16 Di; 68.55 Bd

Introduction

In recent years there has been an increasing interest in ultrathin organic layers such as self assembling- and LB-films or films grown by organic molecular beam epitaxy (OMBE) [1–3]. These films represent a novel class of materials with potential application in advanced optical and electronic systems [4]. On the other hand there exist only a few surface techniques capable to probe the properties of molecular monolayers. Among these techniques only scanning tunneling microscopy and, with some restrictions atomic force microscopy, are able to produce real space images of molecules on surfaces, that means that it gives not only an averaged information of a larger area but the detailed structure of the organic film including point defects, dislocations and grain boundaries [5].

For high resolution molecular imaging by STM the adsorbates must be immobilized, either by a strong interaction with the substrate or by close packing in a 2-*D*-lattice. Therefore ordered organic monolayers on weak interacting substrates are ideal systems to study the image contrast in STM images of organic adsorbates. Several models have been proposed to explain the observed STM image contrast of molecules, but the underlying mechanisms are still under discussion [6–8]. The systematic study presented in this work allows us to discriminate between these different models and to develop a new approach based on the influence of a molecular pseudopotential.

PTCDA and PTCDI have been chosen for several reasons: they are commercially available photochemically stable dye pigments which show sufficient thermal stability to allow purification by sublimation techniques and vapor deposition by molecular beam expitaxy. The molecular structure is shown in Fig. 1. As crystals they are organic semiconductors with potential application in molecular electronics [9]. Monolayers of PTCDA were studied by NEXAFS and ARUPS on Si(111) and Ag(111) and by X-ray diffraction and TEM on cleaved NaCl and KCl crystal surfaces [10–12]. On graphite the crystalline structure of PTCDA is known from the monolayer to the multilayer regime from STM, LEED and X-ray diffraction investigations [13].

In this work we will show how different substrates and changes in the functional groups influence the epitaxial growth and the STM image contrast of PTCDA.

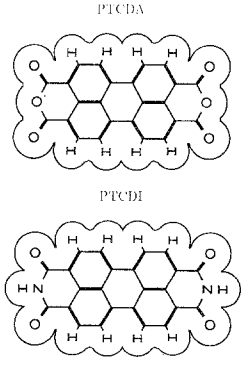

Fig. 1. Molecular structure of PTCDA and PTCDI

Experimental methods

The STM investigations were carried out with a specially developed Video-STM producing images in the constant height mode up to a scanning speed of 20 frames/s. Besides the possibility to image dynamic phenomena, the main advantage of the high scanning speed is, that the signal information is transferred to higher frequencies where the $1/f$-noise of the tunneling current is strongly reduced. In combination with a fast signal averager the instrument is able to produce high resolution images even at extremly noisy conditions. For scanning tunneling spectroscopy (STS) we scan with 1 kHz sweep rate in x-direction while switching the sample voltage from scan to scan between the normal constant height mode and a voltage ramp. In this way we get simultaneously a line scan of the overlayer and the tunneling spectra of each point of the scan. All STM measurements were carried out with Pt-Ir tips in air at room temperature. All images presented in this paper represent unfiltered raw data without any further computer processing.

The MoS_2 was used in form of small lamellae cleaved from selected natural single crystals of different origin. Graphite single crystals were kindly provided by Dr. A. Moore (Union Carbide Comp.).

PTCDA and PTCDI were purified by temperature-gradient sublimation techniques by Prof. N. Karl, Kristallabor Stuttgart. The purity was checked by mass spectrometry and estimated to $\geqq 99\%$. For organic molecular beam epitaxy the material was evaporated from a graphite crucible at a pressure of $\leqq 10^{-7}$ mbar. Before evaporation the freshly cleaved substrate was heated to 200 °C to desorb contaminations. Typical evaporation rates were 20 Å/min at an evaporation temperature of 420 °C and a substrate temperature between 70 and 130 °C. The film thickness was controlled by a quartz crystal microbalance.

Results

PTCDA *on graphite and* MoS_2

On layered materials with large flat regions it is possible to turn to the constant height mode even at larger scan sizes. Figure 2 shows a characteristic 600 Å × 600 Å constant height image of PTCDA on MoS_2 with three islands of different orientation recorded with a scanning speed of 5 frames/s and averaged over 4 frames. As expected for the epitaxial growth on a substrate with six symmetry equivalent directions we found this multi-domain structure on all systems investigated in this work. The average domain size is in the range of 100 Å to 500 Å and does not vary significantly with the evaporation rate in the range 5 Å/min to 50 Å/min or the substrate temperature during evaporation in the range 20–130 °C. The ordered monolayers are always disturbed by defects, dislocations and impurities, as can be seen in Fig. 2. In the video-sequence, one can see complete islands floating around. With our Video-STM it is also possible to see individual molecules appearing and disappearing at the domain edges.

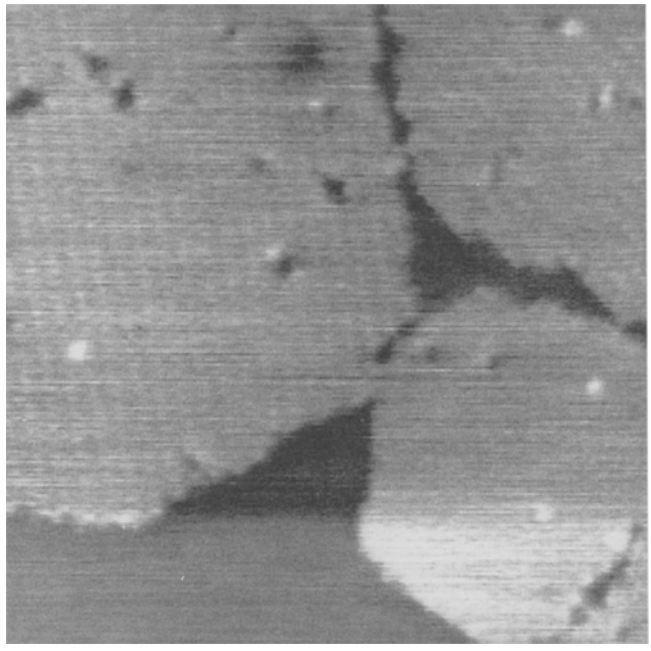

Fig. 2. Large area constant height image of PTCDA on MoS_2. In the video sequence one can see complete islands floating around, keeping their orientation to the substrate. (600 Å × 600 Å, $U = 0.9$ V, $I = 0.6$ nA, 5 frames/s, 4 frames averaged)

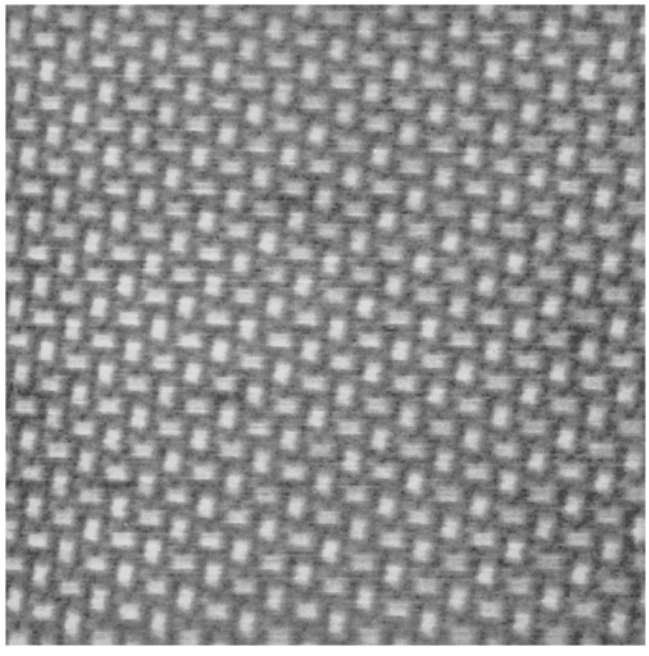

Fig. 3. Low resolution 300 Å × 300 Å image of PTCDA on MoS_2 showing the typical herringbone structure. It was seldom possible to image defect free areas of this size. ($U = 1.2$ V, $I = 0.4$ nA, 5 frames/s, 4 frames averaged)

Figure 3 shows a 300 Å × 300 Å image of PTCDA on MoS_2 with the typical herringbone structure of the overlayer as it is known from the bulk structure and from monolayers on graphite [13, 14]. But unlike to graphite, where we observe a superstructure (Fig. 4, every third

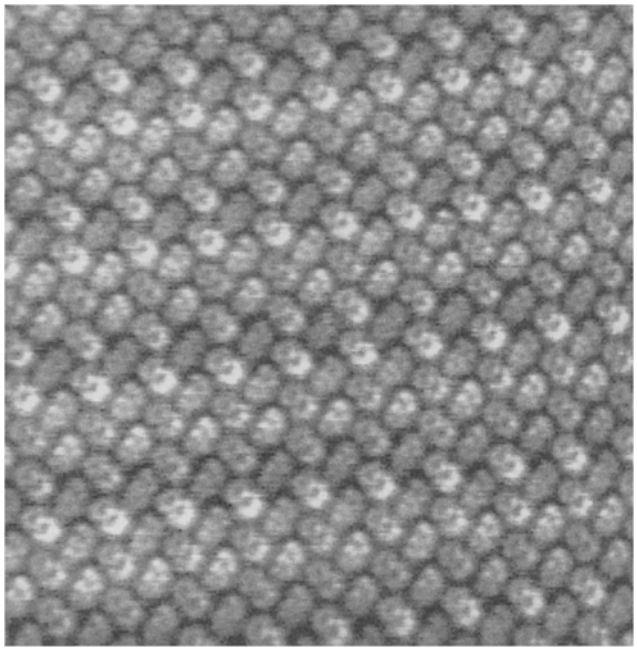

Fig. 4. High resolution image of PTCDA on graphite. In y-direction every third row is brighter. (200 Å × 200 Å, $U = 0.3$ V, $I = 1$ nA, 5 frames/s, 16 frames averaged)

row is brighter) we do not find any superstructure on MoS_2 even at larger area scans.

To determine the crystallographic structure of the overlayers relative to the substrate, we decreased the tunneling resistance until the tip touched the organic films and thereby dragged the molecules away. In this way the underlaying substrate lattices became visible providing the scale for calibration. Thus the lattice constants $\bar{a}$, $\bar{b}$, the angle Γ and the relative orientation Φ of the two-dimensional unit cells of PTCDA and PTCDI could directly be determined by comparison with the translational periods $\bar{g}_1$ and $\bar{g}_2$ of the substrate lattices.

The decision whether the observed overlayers are coincident with the substrate or not depends on the scanned area and the lateral resolution. In Fig. 4 these values are for example 200 Å and 2 Å, respectively. A visible superstructure indicates commensurability in that direction. In this case fractional numbers are entered in Table 1. If no superstructure is observed we cannot decide whether the monolayer is commensurable or not and we use rounded decimal values.

Figure 5a and b show the structural models of the ordering of PTCDA on graphite and MoS_2 as obtained from our STM images. The rectangles mark the unit cells of the ordered epilayers. The arrows in the upper right corner represent the lattice vectors of graphite and MoS_2, respectively. The molecules form a close packed two-dimensional crystal with two molecules per unit cell, which show an atomic overlap for common van der Waals radii. The crystallographic parameters calculated from these models are summarized in Table 1.

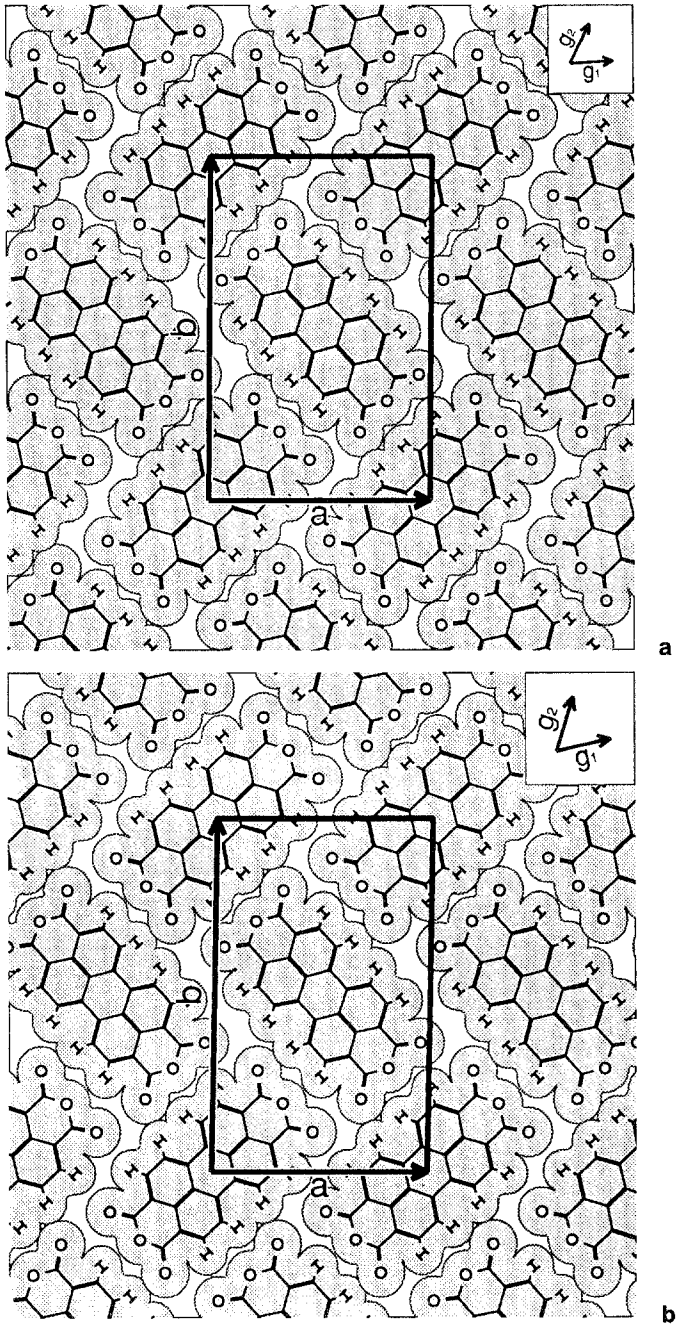

Fig. 5. Structural model of the ordering of a PTCDA monolayer on **a** HOPG and **b** MoS_2. Only one of the six equivalent domains is shown

PTCDI *on graphite and* MoS_2

Figure 6 shows a 400 Å × 400 Å image of PTCDI on MoS_2. The image was recorded in the slow scan constant height mode with a tunneling resistance higher than $10^9\,\Omega$. The three terraces of different brightness in the image are separated by steps of about 3 Å height, which corresponds to the thickness of a monolayer. At a higher resolution the dark upper right part of the image clearly shows the MoS_2 lattice. The areas with medium and high brightness are the first and second layer, respectively. As can be seen from this image the second layer has the same

Table 1. Collection of the unit cell parameters of PTCDA and PTCDI monolayers on HOPG and MoS_2

	HOPG $\lvert\mathbf{g}_1\rvert = 2.46$ Å	MoS_2 $\lvert\mathbf{g}_1\rvert = 3.16$ Å
PTCDA		
a	12.7 Å	12.4 Å
b	19.2 Å	19.7 Å
$\lvert\mathbf{a}\times\mathbf{b}\rvert$	244.6 Å^2	245.0 Å^2
Molecules per unit cell	2	2
$\Gamma = \angle(\mathbf{a}, \mathbf{b})$	89.5°	88.8°
$\Phi = \angle(\mathbf{a}, \mathbf{g}_1)$	3.2°	12.7°
Superstructure	$\begin{pmatrix} 5\frac{1}{3} & -\frac{1}{3} \\ -4 & 9 \end{pmatrix}$	$\begin{pmatrix} 4.3 & -1 \\ -2 & 7 \end{pmatrix}$
Ordering caused by	Herringbone structure Quadrupole moment	
PTCDI		
a	14.5 Å	14.5 Å
b	16.9 Å	17.2 Å
$\lvert\mathbf{a}\times\mathbf{b}\rvert$	243.7 Å^2	247.9 Å^2
Molecules per unit cell	2	2
$\Gamma = \angle(\mathbf{a}, \mathbf{b})$	83.6°	83.1°
$\Phi = \angle(\mathbf{a}, \mathbf{g}_1)$	12.7°	10.9°
Superstructure	$\begin{pmatrix} 6\frac{1}{2} & -1\frac{1}{2} \\ -1\frac{1}{2} & 7\frac{1}{2} \end{pmatrix}$	$\begin{pmatrix} 5 & -1 \\ -1.3 & 6 \end{pmatrix}$
Ordering caused by	Rows Hydrogen bonds	

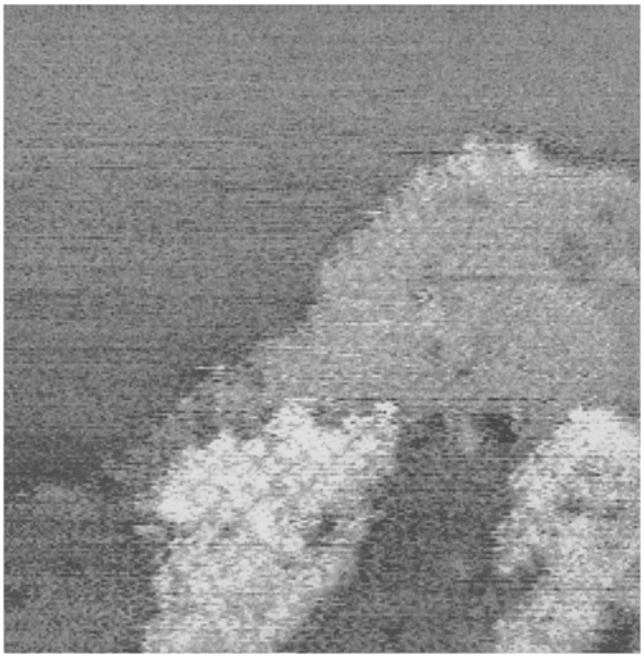

Fig. 6. Slow scan constant current image of PTCDI on MoS_2. The dark area in the upper left part is the MoS_2 substrate. The areas with medium and high brightness represent the first and second layer, respectively. (400 Å × 400 Å, $U = 1.2$ V, $I = 0.3$ nA, 0.1 frames/s, not averaged)

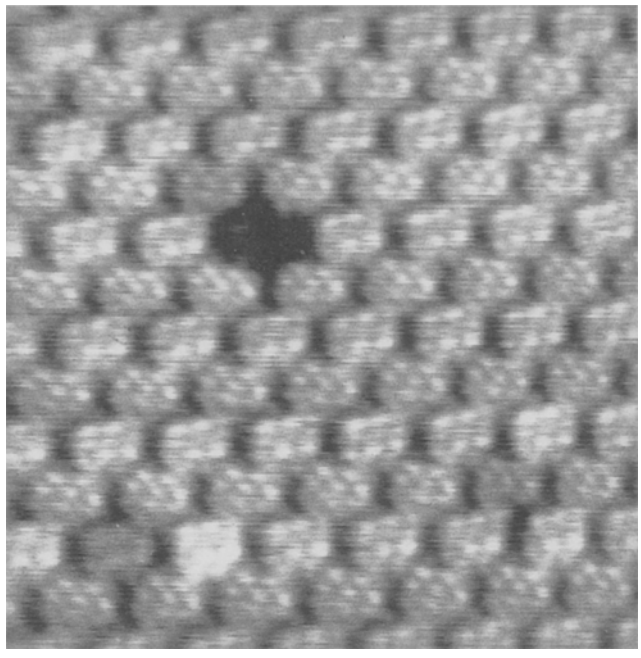

Fig. 7. Constant height image of PTCDI on MoS_2 with a point defect demonstrating the high resolution acieved in this image. (100 Å × 100 Å, $U = 1.0$ V, $I = 4.3$ nA, 5 frames/s, 8 frames averaged)

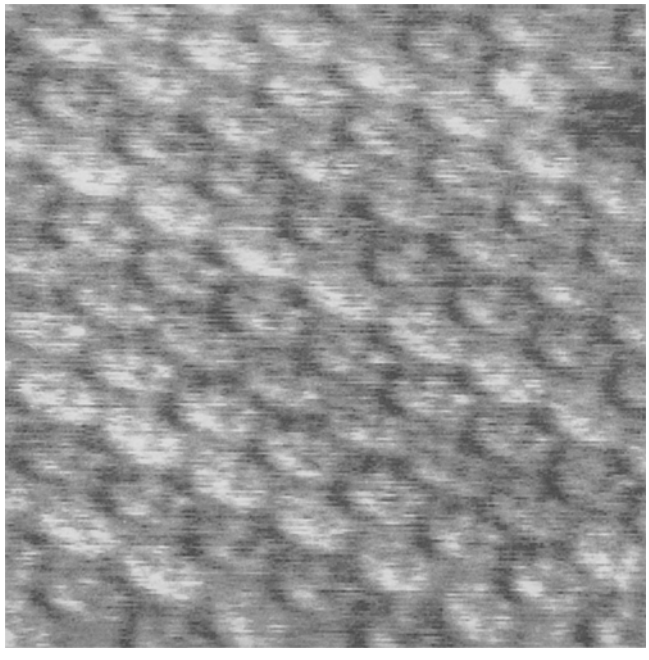

Fig. 8. 100 Å × 100 Å image of PTCDI on graphite showing the typical row like structure. ($U = 0.9$ V, $I = 0.4$ nA, 5 frames/s, 4 frames averaged)

orientation as the first one and the growth starts before the monolayer is closed. We can't image the second layer with a resolution required to determine the size of the unit cell, what is a general experience we made by all systems investigated in this work. Obviously the second layer is bound weaker than the first layer and dragged away during the lowering of the tip.

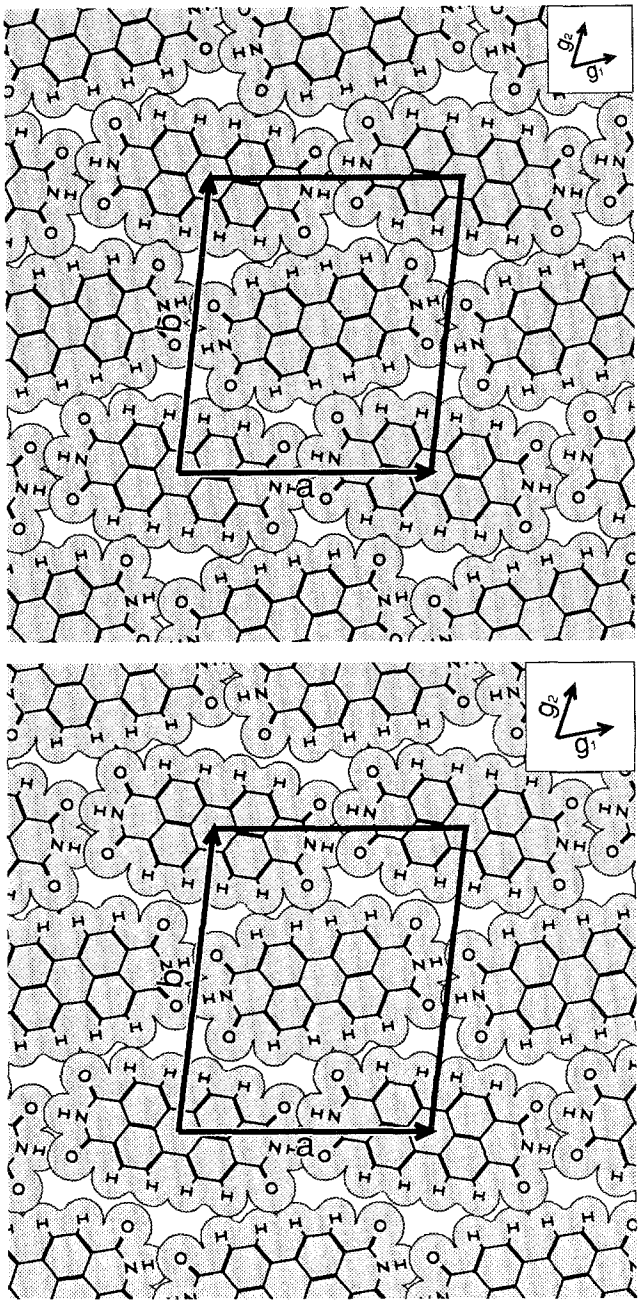

Fig. 9. Structural model of the ordering of PTCDI monolayers on **a** HOPG and **b** MoS_2. Due to hydrogen bonds the molecules show a large overlap along the rows

As in the case of PTCDA, reducing the tunneling resistance leads to high resolution images of the PTCDI monolayers from which it is possible to define the lattice parameters in the way mentioned above. From Fig. 7 we find for PTCDI on MoS_2 $\bar{a}=14.5$ Å, $\bar{b}=17.2$ Å, $\Gamma=83.1°$ and $\Phi=10.9°$ and for the area of the unit cell $\bar{a}\times\bar{b}=247.9$ Å^2. Like PTCDA, PTCDI forms an overlayer on MoS_2 which in one direction shows no commensurability with the underlying substrate lattice. Besides the periodic row like structure Fig. 7 shows a point defect demonstrating the high resolution achieved in this image. The edges of the defect have a width of about 1 Å and are a little bit smaller in the y-direction than in the x-direction showing the limited bandwidth of the tunneling current amplifier of 500 kHz. Any kind of filtering would broaden the edge width. The adjacent unit cells around the point defect have the same size as the "2-D-bulk" unit cells. The intermolecular forces seem to be sufficiently strong to fix the molecules at their position even in the surrounding of a defect.

For PTCDI on graphite from Fig. 8 we obtain the lattice parameters: $\bar{a}=14.5$ Å, $\bar{b}=16.9$ °A, $\Gamma=83.6°$, $\Phi=12.7°$. Figure 9 illustrates the arrangement of PTCDI on HOPG and MoS_2. In the $\bar{a}$-direction the unit cells have the same size on both substrates, whereas the $\bar{b}$-vector on MoS_2 is slightly stretched compared to HOPG.

Image contrast

As already described in a previous article PTCDA on graphite appears in high reslution STM images as a pattern of 10 bright spots [13]. Figure 10a–d show high resolution images of PTCDA and PTCDI on HOPG and MoS_2 all recorded under similar conditions. The achieved resolution strongly depends on the tunneling resistance. All high resolution images of Fig. 10 were recorded in the middle of a larger defect free island with a tunneling distance close to the critical value, where the tip destroys the film. In all four images the molecules appear as six smaller and four brighter spots. In each image one individual molecule correspondingly is marked by 10 cycles, to emphasize the equivalent patterns. The periodic array and the point defect of Fig. 7 allows us to correlate the bright spots clearly to the molecular structure (Fig. 10e). A rotation of the molecular structure by 90° obviously would not fit to the observed tunneling current maxima, which is also evident from Fig. 10e.

The dianhydride and diimide groups are neither visible in all cases nor do they influence the position of the intramolecular tunneling current maxima. The observed pattern of ten bright spots is not influenced by the weakly interacting substrates. The image contrast of an individual molecule does not depend significantly on the tunneling voltage in the range ± 0.3 V to ± 1.0 V on HOPG and $+0.5$ V to $+1.5$ V on MoS_2 sample bias. For negative polarity MoS_2 shows a rectifying behavior. The polarity independence is illustrated in Fig. 11, which shows two simultaneously recorded images of PTCDA on HOPG, one taken with a sample bias of -550 mV and one with $+450$ mV. The bias was switched from line scan to line scan between the two polarities and each polarity was stored in one channel of the frame buffer.

Besides the observed inner structure there are two additional spots between the molecules in the case of PTCDI on MoS_2 (see Fig. 10d). A comparison to the molecular structure of the PTCDI layer is given in Fig. 10e. These two spots are at the positions of the hydrogen bonds.

In addition to the inner structure of individual molecules in Fig. 10 it can be seen, that in the case of PTCDA on graphite and PTCDI on MoS_2 the two molecules per unit cell show different brightness. In all proposed models of Figs. 5 and 9 the two molecules per unit cell are sym-

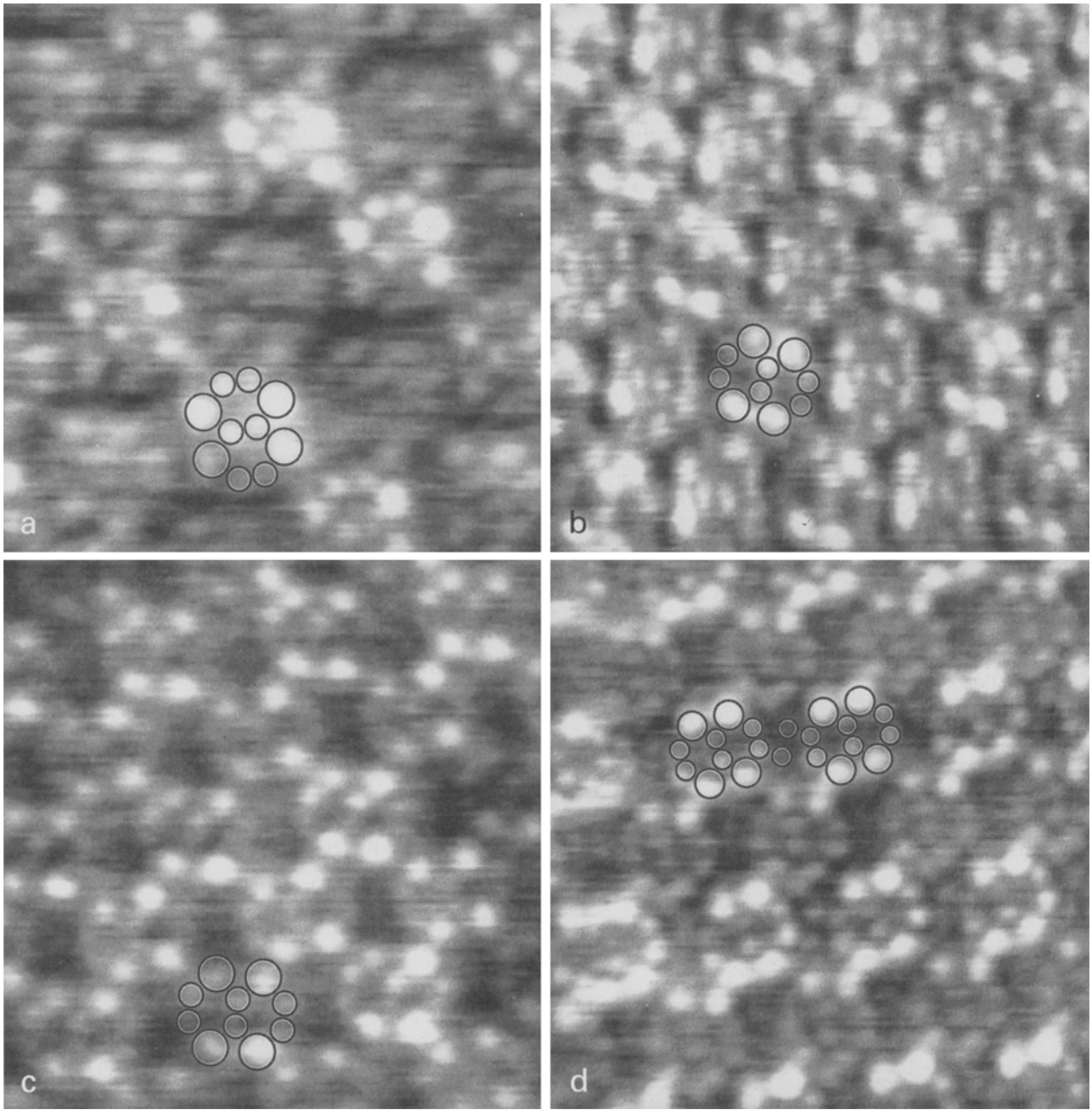

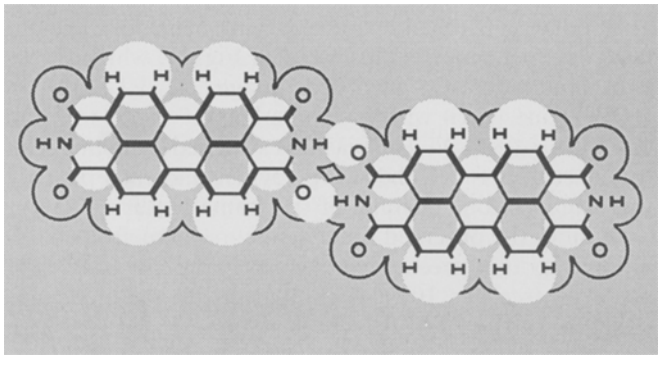

Fig. 10a–e. Comparison of the submolecular resolved images obtained from the four systems under investigation. The observed inner structure of the molecules is similar in all cases. **a** PTCDA on graphite; **b** PTCDA on MoS_2; **c** PTCDI on graphite; **d** PTCDI on MoS_2 (All images: 50 Å × 50 Å, tunneling resistance $3\text{–}5 \times 10^8\ \Omega$, 5 frames/s, 8 frames averaged). **e** Correlation between the observed tunneling current maxima in the high resolution images and the molecular structure. Additional to the innermolecular structure for PTCDI on MoS_2 it was possible to resolve intermolecular bonds

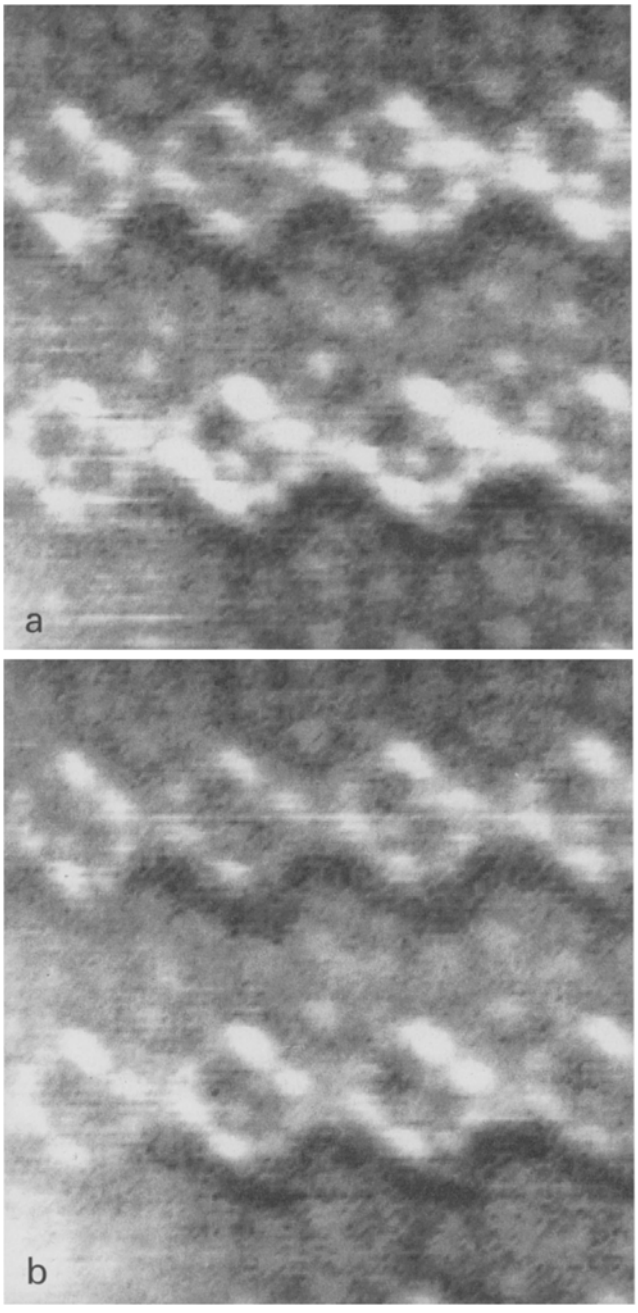

Fig. 11a, b. Independence of the image contrast on the polarity. Simultaneously recorded images of PTCDA on HOPG. **a** Sample bias -550 mV, **b** $+450$ mV

metry equivalent if only the monolayer is taken into account. On the other hand in the adsorbate-substrate complex the two molecules per unit cell see different configurations of substrate atoms. This leads to different brightness only in the two systems PTCDA/HOPG and PTCDI/MoS_2. In the other two cases the different orientation with respect to the substrate has no influence on the observed brightness. In general this means that higher order commensurability can but need not lead to an observable superstructure in the overlayer. In the images 4, 8 and 10 the molecules appear less bright on one side.

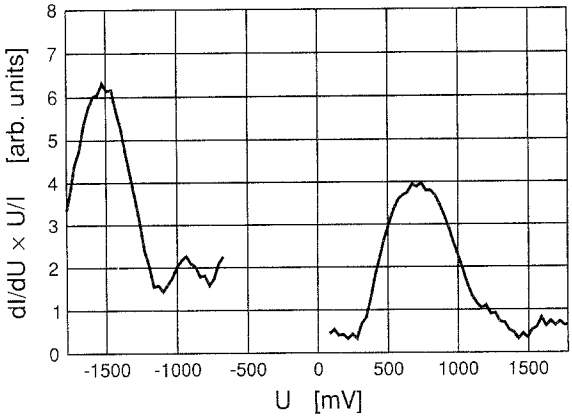

Fig. 12. Normalized conductance vs. voltage of a monolayer PTCDA on graphite

This apparently is caused by the substrate influence evidenced by the superstructure, which leads to a modulation of the tunneling probability or a slight tilt of the molecules.

For a more quantitative analysis of the voltage dependence we performed scanning tunneling spectroscopy experiments in the voltage range ± 1.5 V where we obtain stable images of the overlayers. Figure 12 shows as a preliminary result the normalized conductance vs. voltage curve for PTCDA on HOPG. The curve has two maxima at about $+0.7$ V and -1.5 V. The energy gap corresponding to the distance of the maxima is about 2.2 eV, which is in satisfactory agreement with the singlet exciton energy of 2.2 eV measured at metal/PTCDA/metal devices [15].

Discussion

Epitaxy

In Table 1 the crystallographic results of our STM study are summarized. On both substrates the molecules lie flat on the substrate surface and their arrangement is controlled by intermolecular forces between the polar sidegroups.

For PTCDA on both substrates the quadrupole moment leads to a closely packed herringbone structure with nearly rectangular unit cells [13]. Under these constraints there is only little room for structural variability. The area of the unit cell on HOPG is 244.6 $Å^2$ and on MoS_2 it is 245.0 $Å^2$. At a nearly constant area the unit cell on MoS_2 is only slightly sheared in comparison to graphite (see Fig. 5). From that model we assume that in both cases the $\bar{b}$-direction is commensurate with the underlying substrate, while in the $\bar{a}$-direction on HOPG every third PTCDA molecule is coincident (superstructure) and on MoS_2 this direction shows no commensurability.

The row like structure formed by the PTCDI molecules on HOPG and MoS_2 is caused by hydrogen bonds between the molecules as can be seen from Fig. 9. This intermolecular interaction fixes the values of the $\bar{a}$-axis on both substrates to 14.5 Å. Compared to MoS_2 the unit

cell on graphite is slightly stretched perpendicular to the rows. As in the case of PTCDA, the PTCDI monolayer coincides with the HOPG lattice, but shows no commensurability to MoS_2.

PTCDA has a unique crystal structure in that the two symmetry equivalent molecules lie flat on the (102) plane and form stacks with strong π-electron interaction in the third dimension. Two modifications, α and β, with slightly different unit meshes of the crystal structure are known [12, 14]. A comparison of the lattice parameters of PTCDA crystals with that of the PTCDA monolayers shows, that the molecules form nearly the (102) crystal plane in monolayers on both substrates.

To our knowledge, the crystal structure of PTCDI is not known.

Image contrast

In Fig. 10 all four molecule-substrate combinations show the same intramolecular tunneling current maxima, which leads to the conclusion, that the perylene cores of the molecules dominate the image contrast and that the electronic structure of this core is nearly undisturbed by the substrates. This is an important condition for comparison with theoretical considerations.

First, the observed inner structure can not be explained by local density of state arguments. All tunneling current maxima are at positions with lower electron density. The four brighter spots are at the positions of the electropositive hydrogen atoms, the six smaller spots correspond to the six longest C-C bonds in the molecule. In the Hückel MO-theory a longer bond as well as the electropositive character of hydrogen corresponds to lower electron densities, which is in this model equivalent to an increased pseudopotential at these positions. Preliminary MO calculations confirm these considerations [16]. In the calculated HOMO the maxima do not correspond to the observed tunneling current maxima, which instead coincide with the HOMO wavefunction minima.

In the following we will give two possible explanations for our experimental data:

In a simple three-dimensional model the tunneling probability depends on the height and the width of the barrier and on the kinetic energy of the electrons perpendicular to the barrier. The simplest model for the PTCDA molecules is a box with the dimensions 3 Å high, 14 Å long and 7 Å deep, containing all π-electrons. In such a box the kinetic energy perpendicular to the molecular plane is mainly determined by the height of the box and therefore almost equal for all π-electron states. This means that in this case the tunneling probability depends mainly on the local barrier height the electrons see. At positions with a lower electron density the potential energy of the electrons is higher and the tunneling barrier height therefore reduced. Despite the reduced electron density at these positions, the tunnel current is increased as consequence of the strongly reduced barrier, which influences the tunneling probability exponentially. With a relatively high tunneling resistance between the molecule and the tip, the tunneling from the substrate to the molecule provides an electron reservoir, which seems reasonable because of the much smaller distance between substrate and molecule compared to the molecule-tip distance. This model could explain the observed inner tunneling current distribution of our molecules. At the hydrogen atoms and at the six longest C-C bonds the potential energy of the electrons is higher. At these positions the tunneling barrier to the tip is reduced and thereby the tunneling current increased. It can also explain the fact, that we do not see the underlying substrate through the molecules and why the observed inner structure of the molecules does not depend significantly on the bias voltage or polarity. In our model the visibility of the long H-bridge bonds becomes also reasonable.

Another possible explanation of our images could be the resonant tunneling via molecular orbitals as described by Mizutani et al. [7]. As MO calculations show, the LUMO of PTCDA also is very similar to our observed inner structure [16]. In our scanning tunneling spectroscopy (STM) experiments we found a pronounced maximum for tip negative voltage of about 0.7 eV and a gap of about 2.2 eV. If these maxima correspond to the HOMO and LUMO, respectively, then the fermi level of the substrate is closer to the LUMO. In a resonant tunneling model this could explain why the LUMO contributes more to the tunnel current than the HOMO.

Both models are not able to explain all experimental results. If the tunneling current is dominated by the barrier height one would expect less pronounced maxima in the STS experiments. On the other hand in a resonant tunneling model one would expect a significant influence on the image contrast by changing the tip polarity, which so far has not been observed.

That the maxima of the pseudopotential represent the LUMO, seems to be a general experience in highly delocalized π-electron systems. But for this discussion additional experimental data and detailed theoretical treatments appear necessary.

Conclusions

The results of our work show that there exist well defined preparation conditions which permit epitaxially oriented growth of PTCDA and PTCDI monolayers on graphite and MoS_2. As can be seen from the STM images in all systems under investigation we found well ordered two-dimensional overlayers of flat lying molecules. The detailed crystallographic structure has been determined by comparison of the overlayer with the underlying substrate. On a larger scale all overlayers show a multi-domain structure with many defects. The epitaxial growth is determined by the intermolecular interactions but nearly independent of the substrate. In the submolecularly resolved images the image contrast of individual molecules is dominated by the aromatic perylene system, whereas the substrates do not influence the observed inner molecular structure. In addition to the innermolecular structure of PTCDI it was also possible to image individual intermolecular bonds.

The experimental data can not be explained by density of states arguments instead the observed inner structure qualitatively corresponds to the expected maxima of a single electron pseudopotential. But also the tunneling current distribution resembles the LUMO which is very similar to the pseudopotential. In the STS experiments the monolayers show pronounced maxima with the Fermi-level closer to the LUMO. But since the intramolecular image contrast does not depend on polarity, we expect the influence of the barrier height modulated by the electron pseudopotential to be dominant.

The authors would like to thank Prof. Dr. N. Karl for the highly purified PTCDA and PTCDI and Prof. Dr. E. Sigmund and G. Isenmann for making the MO-calculations available to us. We thank Dr. W. Glatz and Dr. K. Laßmann for helpful discussions. This work was financially supported by the Deutsche Forschungsgemeinschaft under SFB 329.

References

1. Möhwald, H.: Angew. Chem. Adv. Mater. **100**, 750 (1988)
2. Bain, C.D., Whitesides, G.M.: Angew. Chem. Adv. Mater. **101**, 522 (1989)
3. Zimmermann, U., Karl, N.: Surf. Sci. **268**, 296 (1992)
4. Fuchs, H., Ohst, H., Prass, W.: Adv. Mater. **3**, 10 (1991)
5. Chiang, S.: In: Scanning tunneling microscopy. Güntherodt, H.-J., Wiesendanger, R. (eds.). Berlin, Heidelberg, New York: Springer 1992
6. Sautet, P., Joachim, C.: Ultramicroscopy **42–44**, 115 (1992)
7. Mizutani, W., Shigeno, M., Kajimura, K., Ono, M.: Ultramicroscopy **42–44**, 236 (1992)
8. Spong, J.K., Mizes, H.A., LaComb, C.J., Dovek, M.M., Frommer, J.E., Foster, J.S.: Nature **338**, 137 (1989)
9. Forrest, S.R., Leu, L.Y., So, F.F., Yoon, W.Y.: J. Appl. Phys. **66**, 5908 (1989)
10. Zimmermann, U., Schnitzler, G., Karl, N., Umbach, E.: Thin Solid Films **175**, 85 (1989)
11. Umbach, E.: Prog. Surf. Sci. **35**, 113 (1991)
12. Möbus, M., Karl, N., Kobayashi, T.: J. Crystal. Growth **16**, 495 (1992)
13. Ludwig, C., Gompf, B., Glatz, W., Petersen, J., Eisenmenger, W., Möbus, M., Zimmermann, U., Karl, N.: Z. Phys. B**86**, 397 (1992)
14. Lovinger, A.J., Forrest, S.R., Kaplan, M.L., Schmidt, P.H., Venkatesan, T.: J. Appl. Phys. **55**, 476 (1984)
15. Forrest, S.R., Kaplan, M.L., Schmidt, P.H.: J. Appl. Phys. **55**, 1492 (1984)
16. Isenmann, G., Sigmund, E.: Private communication (1993); similar results where obtained by Jung, M., Umbach, E.: (Private communication)